INSTITUTE OF PHYSICS PUBLISHING MODELLING AND SIMULATION IN MATERIALS SCIENCE AND ENGINEERING

Modelling Simul. Mater. Sci. Eng. **12** (2004) 901–915 PII: S0965-0393(04)75507-2

A method for growing multiple cracks without remeshing and its application to fatigue crack growth

Goangseup Zi[1], Jeong-Hoon Song[2], Elisa Budyn[3], Sang-Ho Lee[2] and Ted Belytschko[3]

[1] Department of Civil and Environmental Engineering, Korea University, 5 Ga 1, An-Am Dong, Sung-Buk Gu, Seoul, 136-701, Korea
[2] School of Civil and Environmental Engineering, Yonsei University, 134 Shinchon Dong, Seodaemoon Gu, Seoul 120-749, Korea
[3] Mechanical Engineering, Northwestern University, 2145 Sheridan Rd., Evanston, IL 60208-3111, USA

E-mail: g-zi@korea.ac.kr.

Received 1 February 2004
Published 1 July 2004
Online at stacks.iop.org/MSMSE/12/901
doi:10.1088/0965-0393/12/5/009

Abstract

A numerical model to analyse the growth and the coalescence of cracks in a quasibrittle cell containing multiple cracks is presented. The method is based on the extended finite element method in which discontinuous enrichment functions are added to the finite element approximation to take into account the presence of the cracks, so that it requires no remeshing. In order to describe the discontinuities only the tip enrichment and the step enrichment are used. The method does not require a special enrichment for the junction of two cracks and the junction is automatically captured by the combination of the step enrichments. The geometry of the cracks which is described implicitly by the level set method is independent of the finite element mesh. In the numerical example, linear elastic fracture mechanics is adopted to describe the behaviour of the cracks along with the Paris fatigue law and the intact bulk material is assumed to be elastic. The numerical results show that cracks can grow and interconnect with each other without remeshing as fatigue progresses and that the pattern of fatigue crack development converges with mesh refinement.

1. Introduction

Considerable research has been devoted to obtaining stress intensity factors and the elastic stiffness of materials with arrays of cracks [1, 2] etc. This effort has matured substantially. Recently, Helsing [3] presented a very impressive study of the elastic properties of a unit cell containing ten thousand randomly oriented stationary cracks.

The study of materials with growing arrays of cracks however has been quite limited. Carpinteri and Monetto [4] and Lauterbach and Gross [5] studied crack growth in a brittle material with the boundary element method. Liang *et al* [6] applied the extended finite element method to disordered multiple crack growth in a thin film bonded to an elastic substrate. In [6], the junction of two cracks is not modelled so that a crack tip is not grown further when it approaches another crack very closely. In the work of Budyn *et al* [7], an extended finite element method was developed for growth of multiple cracks based on the critical stress intensity factors. In this paper, that method is modified for fatigue crack growth and applied to problems with two to fifty cracks.

The proposed method is based on the extended finite element method [8, 9], which has been extended to many applications; crack growth with friction [10], arbitrary branched and intersecting cracks [11], three-dimensional crack propagation [12], material discontinuity problems [13], cohesive crack models [14], dynamic fracture problems [15] etc. We show here how the method can be used to model the growth of multiple cracks and to model the junction of cracks. The benefit of using the extended finite element method is that one can model the discontinuities without remeshing.

To illustrate the method, we apply the method to the problem of fatigue crack growth of multiple cracks in a quasi-brittle material. The failure of a quasi-brittle material can be considered to be the consequence of the accumulation of micro-cracks and their interconnection, which results in a complicated load-deflection behaviour [4]. Therefore, the growth and the coalescence of the cracks is of great interest. Under monotonic loading, the material fails as soon as the loading reaches the instability points.

Under cyclic loading with the stress, so that the stress intensity factor is far below the fracture toughness, the material undergoes slow propagation of cracks and, eventually, it fails. We are interested in the estimation of the fatigue life and the failure mechanism of a cell of a quasi-brittle material containing multiple cracks.

We will use linear elastic fracture mechanics and drive the crack growth by the Paris Law (see [16–20] etc). We adopt linear elastic fracture mechanics to describe the behaviour of the cracks and assume that the intact bulk material is elastic. Recently, the cohesive crack model has been studied for fatigue crack growth instead of the linear elastic fracture mechanics [21–23]. Cohesive laws could also be used, as in Zi and Belytschko [14]. However, we will use linear elastic fracture mechanics with the Paris Law for simplicity.

The outline of this paper is as follows. The enrichment for the continuum with multiple cracks is presented in section 2. The weak form and the finite element equations are given in section 3. Section 4 gives the crack growth laws used here. Several numerical examples are given in section 5. Section 6 presents the conclusion of this paper.

2. The enrichment

2.1. The approximation of the displacement field

A domain Ω containing multiple cracks Γ_c is shown in figure 1. The displacement field is continuous for the intact region but discontinuous across the cracks Γ_c. The approximation of the displacement field $\boldsymbol{u}^h$ of the domain is given by

$$\boldsymbol{u}^h = \boldsymbol{u}^0 + \boldsymbol{u}^e \tag{1}$$

where $\boldsymbol{u}^0$ is the continuous displacement field and $\boldsymbol{u}^e$ is the discontinuous (or the enriched) displacement field. The continuous displacement field is approximated by the standard finite

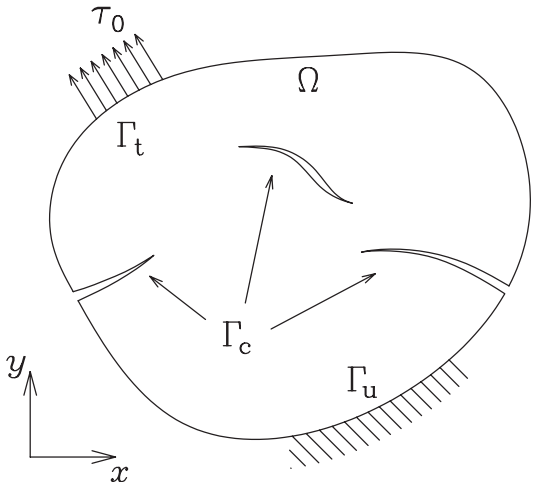

Figure 1. A two-dimensional linear elastic domain containing multiple cracks.

element shape function;

$$\boldsymbol{u}^0 = \sum_{I \in \mathcal{N}} N_I \boldsymbol{u}_I^0 \tag{2}$$

in which $\mathcal{N}$ is the set of nodes, N_I is the shape function of the finite element method and $\boldsymbol{u}_I^0$ is the nodal displacement of node I. The discontinuous displacement field $\boldsymbol{u}^e$, when there is more than one type of enrichment, is given by

$$\boldsymbol{u}^e = \sum_{J \in \mathcal{E}} \boldsymbol{u}^{J,e} \tag{3}$$

where $\mathcal{E}$ is the set of the types of enrichments and $\boldsymbol{u}^{J,e}$ is the displacement enrichment by enrichment type J. The displacement enrichment $\boldsymbol{u}^{J,e}$ is given by

$$\boldsymbol{u}^{J,e} = \sum_{I \in \mathcal{N}_J} N_I \left(\Psi^J - \Psi_I^J \right) \boldsymbol{a}_I^{J,e} \tag{4}$$

where $\mathcal{N}_J$ is the set of the nodes associated with enrichment type J, Ψ^J are the enrichment functions for enrichment type J and $\boldsymbol{a}_I^{J,e}$ are the enrichment parameters. Note that the enrichment function is shifted by its nodal value Ψ_I^J so that the displacement enrichment vanishes at nodal points [14]. As a consequence, $\boldsymbol{u}_I^0$ in (2) is equal to the nodal displacement.

Figure 2 shows an example of the enriched domain. To treat the displacement discontinuity across the crack, the nodes marked by the symbols are enriched. Note that the order of interpolation shape function in (4) does not need to be the same as that in (2) [25]. To obtain a better approximation in the blending elements, we use the quadratic interpolation for (2) and the linear interpolation for (3); therefore for the 6 node triangular elements, we do not use their midpoints for the enrichments [26]. The details of the enrichment function Ψ are given in the following section.

2.2. The enrichment functions

We use only two types of the enrichment functions: the step enrichment and the tip enrichment [13]. When an element is completely cut by a crack, the displacement jump across the crack

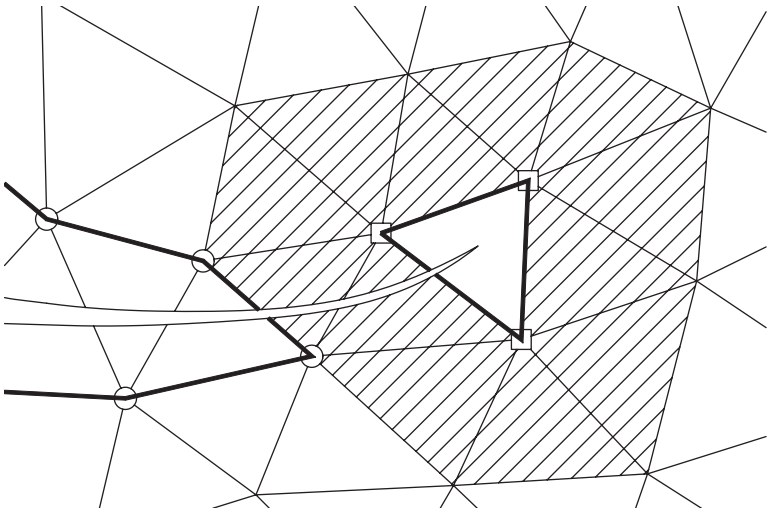

Figure 2. An example of the enriched elements (surrounded by thick lines) and the partially enriched elements (hatched); the circled nodes are enriched by the step enrichment and the squared nodes by the tip enrichment.

is modelled by the step enrichment $\mathbf{\Psi}^{\text{step}}$ which is

$$\mathbf{\Psi}^J = \mathbf{\Psi}^{\text{step}} = \text{sign}(f) \tag{5}$$

in which f is the signed distance function measured with respect to the current crack considered. The position of the crack is defined implicitly by the level set function (see [13, 17, 27]). The line defined by $f = 0$ corresponds to the position of the crack. The function in equation (5) is constant on each side of $f = 0$ with a jump at $f = 0$. The step enrichment has the interesting feature that the enrichment (4) completely vanishes outside the enriched elements due to the shift in (4) [14].

The displacement field for any element containing a crack tip is modelled by the tip enrichment $\mathbf{\Psi}^{\text{tip}}$. The basis functions of the asymptotic solution of a linear elastic crack are used [8]:

$$\mathbf{\Psi}^J = \mathbf{\Psi}^{\text{tip}} = r^{1/2} \times \left\{ \cos\frac{\theta}{2}, \sin\frac{\theta}{2}, \ \cos\frac{\theta}{2}\sin\theta, \sin\frac{\theta}{2}\sin\theta \right\} \tag{6}$$

in which r is the distance from the current crack tip and θ is the angle measured with respect to the tangent at the crack tip. Unlike the step enrichment (5), the tip enrichment does not vanish outside the enriched elements as shown in figure 2.

The partition of unity property holds for the enriched elements surrounded by the thick lines in the figure but it does not hold in the partially enriched elements shaded in the figure, the so called 'blended elements'. The product of the shape function N_I and the enrichment function $\mathbf{\Psi}^J$ increases the order of interpolation in (4). In the blended elements, the partition of unity property does not hold and this can lead to errors (see Chessa *et al* [24]). However, these errors are small for the rapidly decaying asymptotic field and vanish for the step function.

The junction of two cracks occurs when one crack approaches and eventually touches the other (figure 3). The tip enrichment of the approaching crack is removed after the two cracks join, and the connection of two cracks is modelled by a junction enrichment. The enrichment for the nodes whose supports are cut by two or more discontinuities was proposed by Daux *et al* [11].

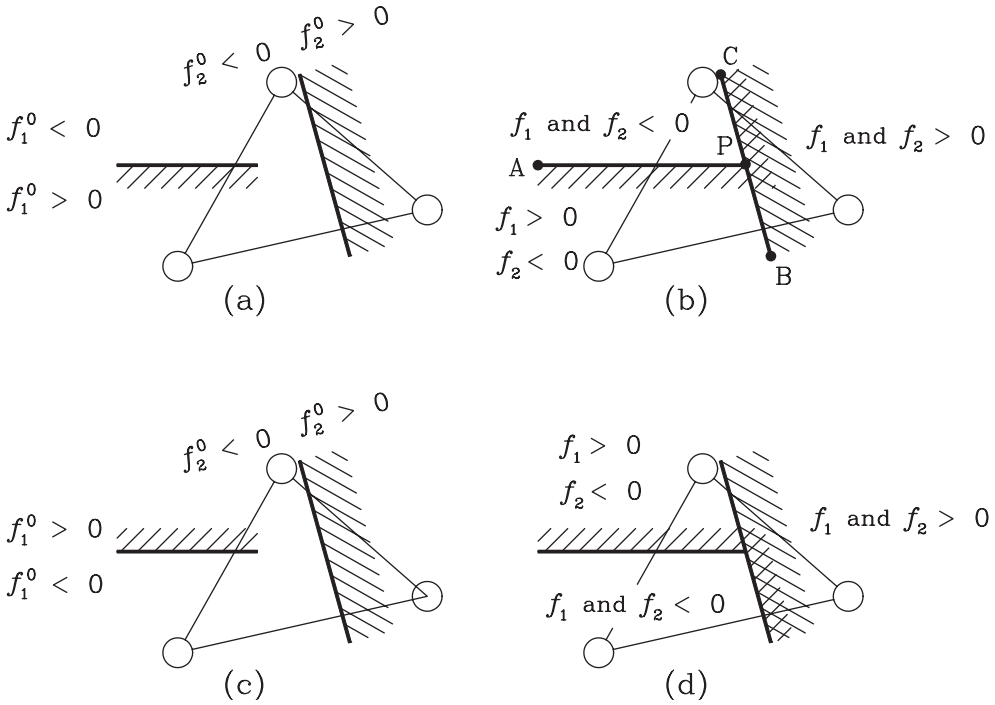

Figure 3. Two cases of sign functions for junction of two cracks, in which crack 1 is approaching crack 2; the signs of the signed distance function of crack 1 before and after junction are shown in (*b*) and (*d*); sign distance functions f are positive in the shaded side.

We found that the junction of two cracks can be implemented more easily by the combination of two step enrichments [28]. For this enrichment, the signed distance function of the approaching crack is changed as shown in figures 3(*b*) and (*d*). For example, in figure 3, we consider two cracks: crack 1 is approaching crack 2. The sign distance function of crack 1, f_1, is calculated by using the line $\overline{\mathrm{APC}}$ in figure 3(*b*). The signs of f_1 and f_2 are identical in the right side of crack 2. Therefore, there are three different types of domains in figure 3(*b*); ($f_1 < 0,\ f_2 < 0$), ($f_1 > 0,\ f_2 > 0$) and ($f_1 > 0,\ f_2 < 0$). In figure 3(*d*), the three domains are ($f_1 > 0,\ f_2 < 0$), ($f_1 > 0,\ f_2 > 0$) and ($f_1 < 0,\ f_2 < 0$). Therefore the combination of two step function enrichments for cracks 1 and 2 with the change of the signed distance function explained above will yield the displacement field required for the junction of two cracks.

The change of the signed distance function seems complicated because it appears that the signed distance function needs to be recalculated after the junction of the cracks. However the recalculation is not needed. The signed distance function of crack 1 of a point $\boldsymbol{x}$ after the cracks join, $f_1(\boldsymbol{x})$, is easily obtained by the following equation:

$$f_1(\boldsymbol{x}) = \begin{cases} f_1^0(\boldsymbol{x}) & \text{for } f_2^0(\boldsymbol{x}_1) f_2^0(\boldsymbol{x}) > 0 \\ f_2^0(\boldsymbol{x}) & \text{for } f_2^0(\boldsymbol{x}_1) f_2^0(\boldsymbol{x}) < 0 \end{cases} \tag{7}$$

in which f_1^0, f_2^0 represent the signed distance functions of cracks 1 and 2 without consideration of the junction, and $\boldsymbol{x}_1$ is any point on crack 1. Equation (7) means that we take $f_1 = f_1^0$ on the side of crack 2 that is joined by crack 1, and $f_1 = f_2^0$ on the other side of crack 2.

3. Weak form and discretized equations

Let us consider the domain Ω containing multiple cracks Γ_c shown in figure 1. The domain is loaded by the external traction $\boldsymbol{\tau}_0$. It is assumed that the crack surfaces are free of traction, and that the intact bulk material is a linear elastic. The weak form of equilibrium of the system is given by

$$\delta W^{\text{int}} = \delta W^{\text{ext}} \tag{8}$$

where

$$\delta W^{\text{int}} = \int_{\Omega\setminus\Gamma_c} \frac{\partial \delta \boldsymbol{u}}{\partial \boldsymbol{x}} \cdot \boldsymbol{\sigma} \mathrm{d}\Omega \tag{9}$$

$$\delta W^{\text{ext}} = \int_{\Gamma_t} \delta \boldsymbol{u} \cdot \boldsymbol{\tau}_0 \, \mathrm{d}\Gamma. \tag{10}$$

Here, W^{int} is the internal work, W^{ext} is the external work by the traction $\boldsymbol{\tau}_0$ along the traction boundary Γ_t, $\delta \boldsymbol{u}$ is the test function (which vanishes along the displacement boundary Γ_{u}) and $\boldsymbol{\sigma}$ is the stress which is calculated from the trial function $\boldsymbol{u}$.

Following the standard Galerkin procedure, we use the same approximation defined in (1) for both $\delta \boldsymbol{u}$ and $\boldsymbol{u}$. From the weak form (8) and the displacement enrichments (1), one can obtain the discrete equilibrium equation:

$$\boldsymbol{f}^{\text{int}} = \boldsymbol{f}^{\text{ext}}, \tag{11}$$

where

$$\boldsymbol{f}^{\text{int}} = \boldsymbol{K}\boldsymbol{q} = \int_{\Omega\setminus\Gamma_c} \boldsymbol{B}^{\text{T}}\boldsymbol{C}\boldsymbol{B} \, \mathrm{d}\Omega \, \boldsymbol{q}, \tag{12}$$

$$\boldsymbol{f}^{\text{ext}} = \int_{\Gamma_t} \boldsymbol{N}^{\text{T}} \boldsymbol{\tau}_0 \, \mathrm{d}\Gamma. \tag{13}$$

Here, $\boldsymbol{f}^{\text{int}}$ and $\boldsymbol{f}^{\text{ext}}$ are the internal and the external forces, respectively, $\boldsymbol{K}$ is the stiffness matrix, $\boldsymbol{q} = [\boldsymbol{q}_1^T, \boldsymbol{q}_2^T, \ldots, \boldsymbol{q}_{N_{\text{tot}}}^T]^T$, $\boldsymbol{q}_I = [\boldsymbol{u}_I^T, \boldsymbol{a}_I^T]^T$ are the generalized nodal displacements, N_{tot} is the total number of nodes, $\boldsymbol{B}$ is the strain–displacement matrix and $\boldsymbol{C}$ is the elastic modulus matrix. The size of $\boldsymbol{a}_I$ is equal to $n_{\text{dof}} \times \left(n_{\text{step}} + n_{\text{tip}} \times 4\right)$, in which n_{dof} is the number of degrees of freedom of a node (2 in two-dimensional problems) and n_{step} and n_{tip} are the number of step enrichments and tip enrichments of the node, respectively. Note that the tip enrichment (6) consists of 4 basis functions. The $\boldsymbol{B}$ matrix is given by

$$\boldsymbol{B} = \left[\boldsymbol{B}^0 \; \boldsymbol{B}^e\right] \tag{14}$$

where $\boldsymbol{B}^0$, $\boldsymbol{B}^e$ are the classical and the enriched parts, respectively. The $\boldsymbol{B}^0$ and $\boldsymbol{B}^e$ matrices are given by

$$\boldsymbol{B}^0 = \left[\boldsymbol{B}_1^0, \boldsymbol{B}_2^0, \ldots, \boldsymbol{B}_{n_e}^0\right] \qquad \text{and} \qquad \boldsymbol{B}^e = \left[\boldsymbol{B}_1^e, \boldsymbol{B}_2^e, \ldots, \boldsymbol{B}_{n_e}^e\right] \tag{15}$$

$$\boldsymbol{B}_I^0 = \begin{bmatrix} \dfrac{\partial N_I}{\partial x} & 0 \\ 0 & \dfrac{\partial N_I}{\partial y} \\ \dfrac{\partial N_I}{\partial y} & \dfrac{\partial N_I}{\partial x} \end{bmatrix} \tag{16}$$

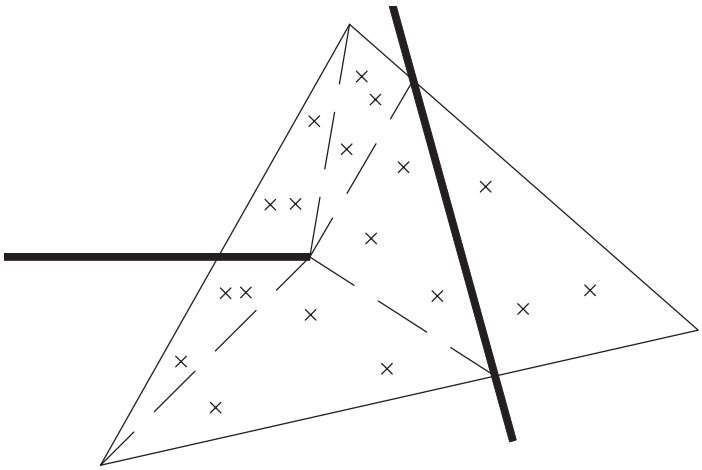

Figure 4. The subdivision of an element containing discontinuities; the thick lines are the discontinuities, the dashed lines the edges of the subdivisions and the crosses are the quadrature points.

$$\boldsymbol{B}_I^e = \begin{bmatrix} \dfrac{\partial N_I}{\partial x}(\boldsymbol{\Psi}^J - \boldsymbol{\Psi}_I^J) + N_I \dfrac{\partial \boldsymbol{\Psi}^J}{\partial x} & 0 \\ 0 & \dfrac{\partial N_I}{\partial y}(\boldsymbol{\Psi}^J - \boldsymbol{\Psi}_I^J) + N_I \dfrac{\partial \boldsymbol{\Psi}^J}{\partial y} \\ \dfrac{\partial N_I}{\partial y}(\boldsymbol{\Psi}^J - \boldsymbol{\Psi}_I^J) + N_I \dfrac{\partial \boldsymbol{\Psi}^J}{\partial y} & \dfrac{\partial N_I}{\partial x}(\boldsymbol{\Psi}^J - \boldsymbol{\Psi}_I^J) + N_I \dfrac{\partial \boldsymbol{\Psi}^J}{\partial x} \end{bmatrix} \qquad \forall J \in \mathcal{E}_I \tag{17}$$

where n_e is the number of the nodes of an element and $\mathcal{E}_I$ is the set of the enrichments of node I. Note that a node can be enriched by more than one enrichment function. Therefore, to construct the strain–displacement matrix $\boldsymbol{B}_I^e$ in equation (17), it is necessary to add all contributions from the set $\mathcal{E}_I$ to the $\boldsymbol{B}$ matrix of the current element. The set $\mathcal{E}_I$ includes all the enrichments of node I.

The differentiation of the enrichment function $\boldsymbol{\Psi}^J$ yields the Dirac delta function at the positions of the cracks Γ_c. However, since the integration domain in (12) excludes the cracks Γ_c, we do not consider the Dirac delta function. For example, the derivative of the step enrichment $\boldsymbol{\Psi}^{\text{step}}$ (5) in (17) is zero.

Since the integral in (12) is discontinuous in the elements containing discontinuities, each element containing any discontinuities is subdivided as shown in figure 4 (see Budyn [28] for more details). The lines of the discontinuities coincide with the edges of the subdivisions. Then the subdivisions are numerically integrated. The subdivision is just for the numerical integration and does not affect the connectivity of the finite element mesh.

4. Description of cracks

4.1. Level sets

Each crack is described implicitly by the signed distance function f^c. The signed distance function $f(\boldsymbol{x})$ is defined as the minimum distance from a point $\boldsymbol{x}$ to the crack Γ_c. Given the nodal values of the signed distance function f_I^c, the signed distance function in the domain Ω

is interpolated by means of finite element shape functions;

$$f^c(\boldsymbol{x}) = \sum_I N_I(\boldsymbol{x}) f_I^c. \tag{18}$$

In addition, the end points of each crack need to be specified to describe the crack geometry. Although other interpolation techniques, such as the moving least squares [29], are available, (18) is the simplest yet that is accurate enough to capture the crack growth. We use the vector level set method developed by Ventura *et al* [17, 30], where a detailed discussion for updating the level set can be found.

4.2. Crack growth law

The fatigue life of structural or mechanical members is defined as the number of loading cycles until the member fails due to crack growth. The fatigue life can be divided into three main periods: crack initiation, crack growth, and finally, overload failure. Here we are interested in the crack growth period. The relation between crack growth and the stress intensity factor in the period of crack growth is almost linear in a log–log plot. Based on experimental observation, Paris and Erdogan [31] developed an empirical formula, which is called the 'Paris Law', for crack growth as a function of stress intensity factor:

$$\frac{\mathrm{d}a}{\mathrm{d}N} = C\,(\Delta K)^m \tag{19}$$

where a is the length of the crack, N is the number of cycles, ΔK is the change of the stress intensity factor during a load cycle and C and m are the fatigue crack growth parameters. For mixed mode fracture problems, K is the equivalent mode I stress intensity factor:

$$K = \sqrt{K_{\mathrm{I}}^2 + K_{\mathrm{II}}^2}. \tag{20}$$

Growing multiple cracks requires that the crack increments be computed for individual cracks for a number of fatigue cycles. For this, we control the size of the crack increment Δa_{ctl} at the crack tip at which ΔK is maximum. Once that crack tip is identified, we calculate the corresponding number of fatigue cycles ΔN with Δa_{ctl} from (19). The crack increment Δa_i of crack tip i is obtained by using the corresponding ΔK_i of the crack tip i and ΔN.

The direction of the crack growth ϑ is determined based on the maximum hoop stress criterion:

$$\vartheta = 2 \arctan \frac{1}{4}\left(\rho_K \pm \sqrt{{\rho_K}^2 + 8}\right) \tag{21}$$

where $\rho_K = K_{\mathrm{I}}/K_{\mathrm{II}}$ is the ratio of the mode I stress intensity factor to the mode II one. The stress intensity factors in (19)–(21) are calculated by interaction integral [9, 32, 33].

4.3. Coalescence of two cracks

When a crack reaches an external boundary Γ or is connected to another crack Γ_c, the topology of the crack changes as shown in figure 5. In these cases, only the step enrichment is retained—the tip enrichment is removed (or 'killed'). If any boundary is found within a distance r_s measured from crack tip i, then we join the crack to the boundary or the crack at point P. The point P on the boundary is the closest point to the previous position of the crack tip as shown in figure 5(a). If the boundary is another crack, P is the midpoint of the closest segment of the crack to the crack tip as shown in figure 5(b).

After two cracks are connected, the strain energy near the connection is anticipated to be very small. Therefore, if any crack tip of Γ_c is found within the distance r_s from the point of the junction, the growth of the crack tip is disabled.

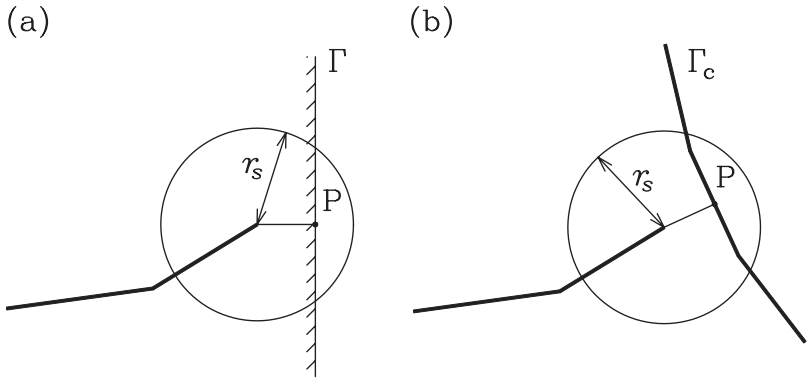

Figure 5. Change of the topology of a crack when it approaches (*a*) a boundary Γ or (*b*) another crack Γ_c, in which the thick lines represent the cracks.

To avoid having boundaries in the annular domain used for the calculation of the *J*-integral [8], the distance r_s is chosen to be greater than or equal to the size l_i of the *J*-integral domain. Therefore,

$$r_s = \max(\Delta a_i,\ l_i). \tag{22}$$

The size of l_i is typically taken as $2h_c$ where h_c is the characteristic size of an element [9]. Note that to avoid the creation of a rigid body mode, if two cracks are already connected to each other, we do not join them again.

If periodic boundary conditions are used, any crack that reaches a boundary must emerge from the image boundary. This can be incorporated in this model but was not done here.

5. Numerical examples

5.1. Centre-cracked and edge-cracked specimens

The verification of the extended finite element method can be found in [8–10, 12]. For completeness of this paper, we present the load–deflection behaviour and the stress intensity factors of two typical fracture specimens shown in figure 6 under plane strain condition. A centre-cracked and an edge cracked specimen are loaded at their top and bottom edges by uniform traction. One node on the bottom edge is pinned, the other is on a horizontal roller.

We use the typical material properties of brittle materials, such as ceramics: Young's modulus $E = 416\,\text{GPa}$, Poisson ratio $\nu = 0.23$ and fracture toughness $K_c = 3.5\,\text{MPa}\sqrt{\text{m}}$. The radius for the calculation of the stress intensity factors by the interaction integral is taken as $2h_c$. To obtain the load–deflection curve in figure 6, the external force is adjusted so that the stress intensity factor is equal to the fracture toughness at the crack tips as the cracks are grown.

It is shown that both stress intensity factors and the load deflection curves of the problems considered agree well with the analytical results found in Tada *et al* [34].

5.2. Growth of 10 fatigue cracks with different mesh refinements

To test the mesh dependency of the method, we calculated the crack propagation patterns for 10 fatigue cracks with three meshes where $h_c = 0.05, 0.06, 0.07$; h_c is the ratio of the average size of an element to the width of the cell. The meshes are shown in figure 7. The cell is squared with

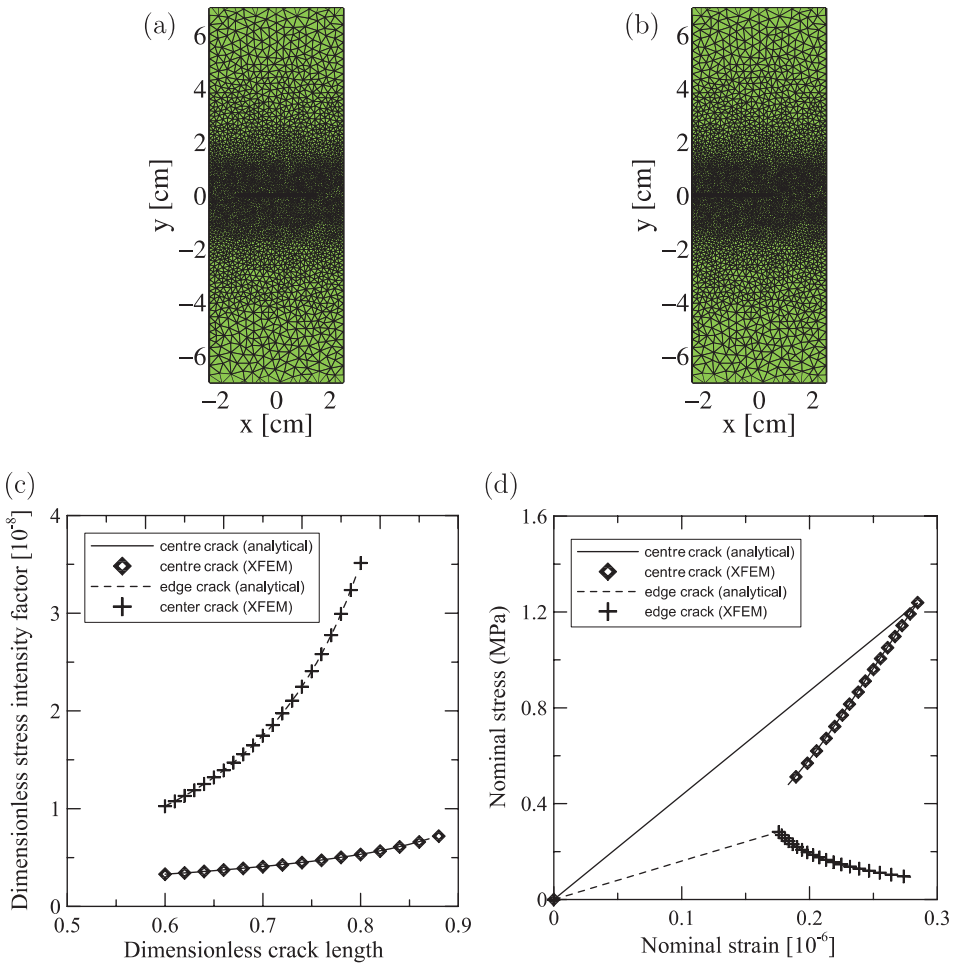

Figure 6. Results for centre crack and edge crack specimens with the meshes for (*a*) centre crack and (*b*) edge crack, (*c*) the stress intensity factors and (*d*) the load deflection curves, in which the stress intensity factor is scaled by $E'\sqrt{\text{width}}$.

(This figure is in colour only in the electronic version)

the side of length 0.2 m. The parameters of the Paris Law are $C = 4.0 \times 10^{-10}$ (MPa $\sqrt{\text{m}}$)$^{-m}$ m and $m = 4$. The cell is loaded by the cyclic traction $t_y = 0$–30 kPa at the bottom and the top edge. The left bottom corner of the cell is fixed and the right bottom corner is supported by a roller.

The corresponding cracking patterns are plotted in the right side of the meshes in figure 7. The cracking patterns with structured cross triangle meshes are also plotted. The cracking patterns with all the meshes agree quite well with each other. Therefore, the mesh dependency of the model appears very low.

5.3. Growth of 50 fatigue cracks

We consider a square plate with 50 initial cracks as shown in figure 8. The material parameters and the loading condition are the same as those with 10 cracks. The positions and the

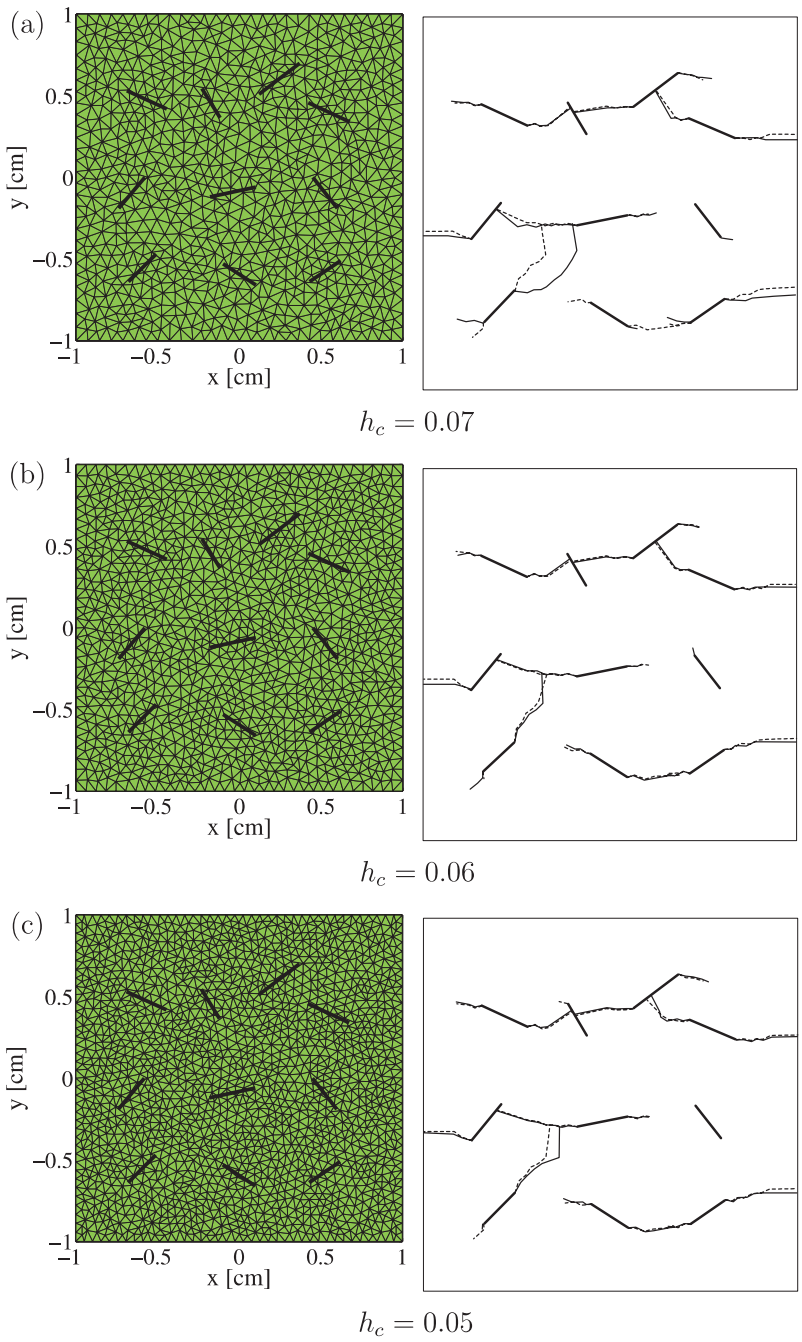

Figure 7. Comparisons of the fatigue crack patterns for different meshes; (*a*) $h_c = 0.07$, (*b*) 0.06 and (*c*) 0.05, in which the thick lines are for the initial 10 cracks, the thin lines for the cracks and the dashed lines for the cracks obtained from the cross triangular meshes with the same mesh refinements.

(This figure is in colour only in the electronic version)

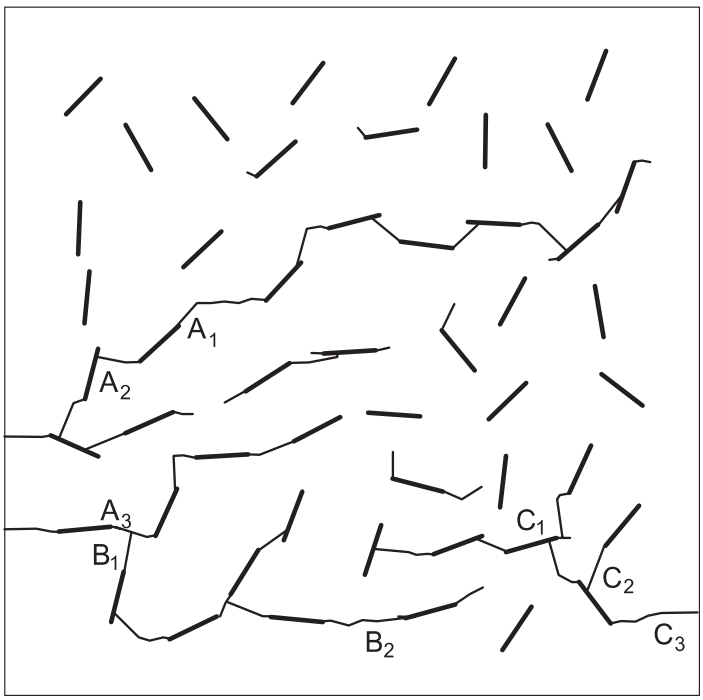

Figure 8. Cell model containing 50 randomly oriented cracks; the thick lines are for the initial cracks and the thin lines represent the growth of the cracks.

orientations of the initial cracks are random. The initial crack lengths are fixed as 1.5 mm and the average element size is $h_c = 0.04$.

Because of the loading direction, some of the cracks do not grow or the amount of the crack growth is negligible compared to others. Fatigue crack growth is most pronounced initially for the cracks placed in the direction of the width of the cell. As fatigue proceeds, the cracks join to form larger cracks. This joining process eventually results in the failure of the cell, i.e. percolation occurs. When a crack coalesces with another larger crack like the cracks near the bottom of the cell, they join approximately at a right angle. This is due to the fact that the stress state near the crack tip gets close to mode I as it approaches another larger crack. This phenomenon was also reported by [6].

The degradation of the elastic stiffness, i.e. $t_y/\Delta V$ in which ΔV is the volume swept by the loading surface, is plotted in figure 9. The stiffness is scaled by the initial value when there is no crack. As fatigue proceeds, the stiffness degrades monotonically and is less than 10% of its initial value for the configuration shown in figure 8. When junction of two cracks occurs, the stiffness degrades rapidly. The labels on figure 9(*a*) correspond to the positions of junction of cracks shown in figure 8. For example, the sudden stiffness degradation at the position of A in figure 9(*a*) is due to three successive junctions A_1, A_2, A_3 in figure 8. A sudden stiffness degradation is observed in the models with 10–40 cracks when two cracks join each other. The rate of the overall stiffness degradation is 7.4 in the log–log plot for this example as shown in figure 9(*b*). We found that the junction significantly affects the overall stiffness degradation.

We also examined how a variable modulus affects the crack growth. This is the type of problem that can be solved by this method but not easily by boundary element methods.

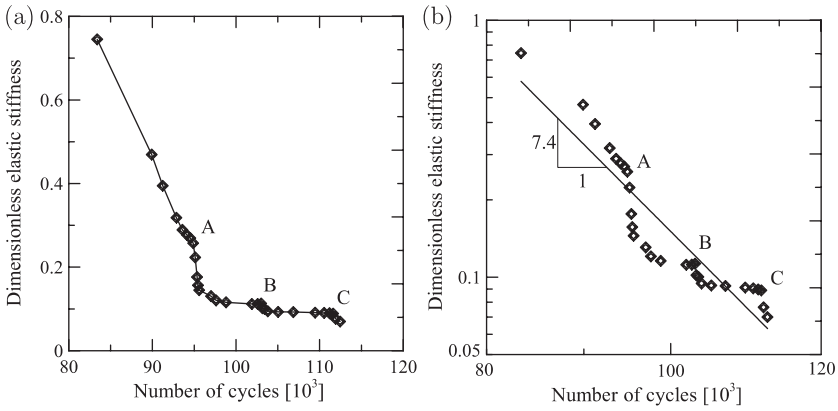

Figure 9. The degradation of the representative modulus of a cell containing 50 randomly oriented cracks as fatigue proceeds, in which the labels A, B, C correspond to the junctions shown in figure 8.

The Young's modulus of the cell is given by

$$E(x, y) = E_0 \left\{ 1 + 0.05 \left[\sin\left(\frac{4\pi x}{W}\right) + \sin\left(\frac{4\pi y}{H}\right) \right] \right\} \tag{23}$$

where E_0 is the reference modulus, W and H are the width and the height of the cell, respectively. The Young's modulus is perturbed 10% from the reference value. The correction for the variable modulus on the stress intensity factor as in [35] is not taken into account although it can be incorporated in this model.

The cracking pattern with the variable modulus is shown in figure 10, in which the change of the modulus is also plotted. The dark region corresponds to high value of the modulus. Compared to figure 8, the cracks in the region with low modulus grow faster than in the case with the homogeneous modulus. It seems that the smooth change of modulus with 10% deviation does not affect the cracking pattern.

6. Conclusions

A method to simulate the fatigue failure of a quasi-brittle material containing multiple cracks has been presented. The method is based on the extended finite element method. To model the change of the displacement by the presence of the linear elastic cracks, the step enrichment and the tip enrichments are used for each crack. A special junction enrichment is not needed to model the junction of two cracks.

The cracks are described implicitly by using the level set method. The position of a crack is identified by the finite element interpolation of the nodal values of the signed distance function measured with respect to the crack. So the geometric description of a crack is completely specified by nodal values of the level set and the positions of the end points.

The simulation with more cracks may require more computational resources. As the number of cracks in a cell increases, so does the mesh refinement required to accurately track it. The computational cost increases almost quadratically.

The numerical examples show that the model can simulate the growth and interconnection and, eventually, percolation of a cell containing multiple cracks without remeshing. The pattern of the fatigue crack development converges with increasing mesh refinement. It is shown that

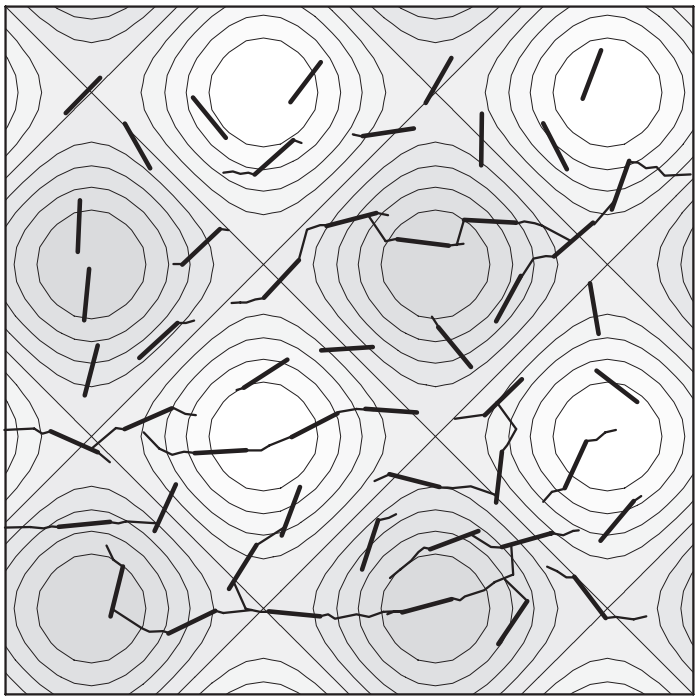

Figure 10. The fatigue crack pattern of a cell containing 50 randomly oriented cracks, in which the thick lines are for the initial cracks and the thin lines the fatigue cracks; the Young's modulus of the specimen gradually changes.

the cracking patterns are almost independent of the mesh when the initial cracks span more than approximately 4 elements.

While boundary element methods can also treat this class of problems, the extended finite element method has the advantage that it can readily be applied to inhomogeneous problems. It can also readily be applied to nonlinear problems, in contrast to boundary element methods.

Acknowledgment

The research grant of Office of Naval Research to Northwestern University is greatly appreciated.

References

[1] Horii H and Nemat-Nasser S 1982 Overall modulus of solids with microcracks: load-induced anisotropy *J. Mech. Phys. Solids* **31** 155–71
[2] Kachanov M 1987 Elastic solids with many cracks–A simple method of analysis *Int. J. Solids Struct.* **23** 23–43
[3] Helsing J 1999 Fast and accurate numerical solution to an elastostatic problem involving ten thousand randomly oriented cracks *Int. J. Fracture* **100** 321–7
[4] Carpinteri A and Monetto I 1999 Snap-back analysis of fracture evolution in multi-cracked solids using boundary element method *Int. J. Fracture* **98** 225–41
[5] Lauterbach B and Gross D 2002 The role of nucleation and growth of microcracks in brittle solids under compression: a numerical study *Acta Mech.* **159** 199–211
[6] Liang J, Huang R, Prevost J H and Suo Z 2003 Evolving crack patterns in thin films with the extended finite element method *Int. J. Solids Struct.* **40** 2343–54

[7] Budyn E, Zi G, Moes N and Belytschko T A method for multiple crack growth in brittle materials without remeshing *Int. J. Numer. Methods Eng.* submitted
[8] Belytschko T and Black T 1999 Elastic crack growth in finite elements with minimal remeshing *Int. J. Numer. Methods Eng.* **45** 601–20
[9] Moës N, Dolbow J and Belytschko T 1999 A finite element method for crack growth without remeshing *Int. J. Numer. Methods Eng.* **46** 131–50
[10] Dolbow J, Moës N and Belytschko T 2000 An extended finite element method for modelling crack growth with friction contact *Comput. Methods Appl. Mech. Eng.* **190** 6825–46
[11] Daux C, Moës N, Dolbow J, Sukumar N and Belytschko T 2000 Arbitrary branched and intersecting cracks with the extended finite element method *Int. J. Numer. Methods Eng.* **48** 1741–60
[12] Sukumar N, Moës N, Moran B and Belytschko T 2000 Extended finite element method for three-dimensional crack modelling *Int. J. Numer. Methods Eng.* **48** 1549–70
[13] Belytschko T, Moës N, Usui S and Parimi C 2001 Arbitrary discontinuities in finite elements *Int. J. Numer. Methods Eng.* **50** 993–1013
[14] Zi G and Belytschko T 2003 New crack-tip elements for XFEM and applications to cohesive cracks *Int. J. Numer. Methods Eng.* **57** 2221–40
[15] Belytschko T, Chen H, Xu J and Zi G 2003 Dynamic crack propagation based on loss of hyperbolicity with a new discontinuous enrichment *Int. J. Numer. Methods Eng.* **58** 1873–905
[16] Fleming M, Chu Y A, Moran B and Belytschko T 1997 Enriched element-free Galerkin methods for crack tip fields *Int. J. Numer. Methods Eng.* **40** 1483–504
[17] Ventura G, Xu J X and Belytschko T 2002 A vector level set method and new discontinuity approximations for crack growth by EFG *Int. J. Numer. Methods Eng.* **54** 923–44
[18] Lawrence M, Liu W K, Besterfield G and Belytschko T 1990 Fatigue crack-growth reliability *J. Eng. Mech.* **116** (ASCE) 698–708
[19] Yuan J L, Wing K L and Belytschko T 1992 A stochastic damage model for the rupture prediction of a multiphase solid. 1. Parametric studies *Int. J. Fracture* **55** 321–40
[20] Liu W K, Chen Y J, Belytschko T and Lua Y J 1996 Three reliability methods for fatigue crack growth *Eng. Fracture Mech.* **53** 733–52
[21] Nguyen O, Repetto E A, Ortiz M and Radovitzky R A 2001 A cohesive model of fatigue crack growth *Int. J. Fracture* **110** 351–69
[22] Roe K L and Siegmund T 2003 An irreversible cohesive zone model for interface fatigue crack growth simulation *Eng. Fracture Mech.* **70** 209–32
[23] Yang B, Mall S and Ravi-Chandar K 2001 A cohesive zone model for fatigue crack growth in quasibrittle materials *Int. J. Solids Struct.* **38** 3927–44
[24] Chessa J, Wang H and Belytschko T 2003 On the construction of blending elements for local partition of unity enriched finite elements *Int. J. Numer. Methods Eng.* **57** 1015–38
[25] Strouboulis T, Copps K and Babuška I 2000 The generalized finite element method: an example of its implementation and illustration of its performance *Int. J. Numer. Methods Eng.* **47** 1401–17
[26] Stazi F, Budyn E, Chessa J and Belytschko T 2003 XFEM for fracture mechanics with quadratic elements *Comput. Mech.* **31** 38–48
[27] Gravouil A, Möes N and Belytschko T 2002 Non planar 3D crack growth by the extended finite elements and the level sets. Part II: Level set update *Int. J. Numer. Methods Eng.* **53** 2569–86
[28] Budyn E 2004 Multiple crack growth by the eXtended Finite Element Method *PhD Thesis* Northwestern University
[29] Belytschko T, Lu Y Y and Gu L 1994 Element-free Galerkin methods *Int. J. Numer. Methods Eng.* **37** 229–56
[30] Ventura G, Budyn E and Belytschko T 2003 Vector level set for description of propagating cracks in finite elements *Int. J. Numer. Methods Eng.* **58** 1571–92
[31] Paris P C and Erdogan F 1963 A critical analysis of crack propagation laws *J. Basic Eng.* **85** 528–34
[32] Yau J, Wang S and Corten H 1980 A mixed-mode crack analysis of isotropic solids using conservation laws of elasticity *J. Appl. Mech.* **47** (ASME) 335–41
[33] Moran B and Shih C 1987 Crack tip and associated domain integrals from momentum and energy balance *Eng. Fracture Mech.* **27** 615–42
[34] Tada H, Paris P C and Irwin G R 1985 *The Stress Analysis of Cracks Handbook* (Hellertown, PA: Del Research Corp.)
[35] Dolbow J E and Gosz M 2002 On the computation of mixed-mode stress intensity factors in functionally graded materials *Int. J. Solids Struct.* **39** 2557–74